

THE BRIGHTEST OF REIONIZING GALAXIES SURVEY: CONSTRAINTS ON THE BRIGHT END OF THE $z \sim 8$ LUMINOSITY FUNCTION*

L.D. BRADLEY¹, M. TRENTI^{2,3,†}, P.A. OESCH^{4,‡}, M. STIAVELLI¹, T. TREU⁵, R.J. BOUWENS⁶, J.M. SHULL⁷,
 B.W. HOLWERDA⁸, N. PIRZKAL¹

Accepted to The Astrophysical Journal

ABSTRACT

We report the discovery of 33 Lyman break galaxy (LBG) candidates at $z \sim 8$ detected in *Hubble Space Telescope* (*HST*) Wide Field Camera 3 (WFC3) imaging as part of the Brightest of Reionizing Galaxies (BoRG) pure-parallel survey. The ongoing BoRG survey currently has the largest area (274 arcmin²) with Y_{098} (or Y_{105}), J_{125} , and H_{160} band coverage needed to search for $z \sim 8$ galaxies, about three times the current CANDELS area, and slightly larger than what will be the final CANDELS wide component with Y_{105} data (required to select $z \sim 8$ sources). Our sample of 33 relatively bright Y_{098} -dropout galaxies have J_{125} band magnitudes between 25.5 and 27.4 mag. This is the largest sample of bright ($J_{125} \lesssim 27.4$) $z \sim 8$ galaxy candidates presented to date. Combining our dataset with the Hubble Ultra-Deep Field (HUDF09) dataset, we constrain the rest-frame ultraviolet galaxy luminosity function at $z \sim 8$ over the widest dynamic range currently available. The combined datasets are well fitted by a Schechter function, i.e. $\phi(L) = \phi_*(L/L_*)^\alpha e^{-(L/L_*)}$, without evidence for an excess of sources at the bright end. At 68% confidence, for $h = 0.7$ we derive $\phi_* = (4.3_{-2.1}^{+3.5}) \times 10^{-4}$ Mpc⁻³, $M_* = -20.26_{-0.34}^{+0.29}$, and a very steep faint-end slope $\alpha = -1.98_{-0.22}^{+0.23}$. While the best-fit parameters still have a strong degeneracy, especially between ϕ_* and M_* , our improved coverage at the bright end has reduced the uncertainty of the faint-end power-law slope at $z \sim 8$ compared to the best previous determination at ± 0.4 . With a future expansion of the BoRG survey, combined with planned ultradeep WFC3/IR observations, it will be possible to further reduce this uncertainty and clearly demonstrate the steepening of the faint-end slope compared to measurements at lower redshift, thereby confirming the key role played by small galaxies in the reionization of the universe.

Subject headings: cosmology: observations — galaxies: evolution — galaxies: formation — galaxies: high-redshift

1. INTRODUCTION

Finding the earliest galaxies in the universe and characterizing their properties and contribution to the reionization of the universe are some of the most important goals of extragalactic astronomy. The Wide Field Camera 3 (WFC3) aboard the *Hubble Space Telescope* (*HST*) has significantly expanded the high-redshift frontier with the

detection and study of galaxies at $z \gtrsim 7$. The ultradeep WFC3/IR observations of the Hubble Ultra-Deep Field (HUDF09) and nearby fields have so far yielded 73 $z \sim 7$ and 59 $z \sim 8$ Lyman-break galaxy (LBG) candidates (Bouwens et al. 2011b, see also Lorenzoni et al. 2011; McLure et al. 2011), including one at $z \sim 10$ (Bouwens et al. 2011a). These ultradeep observations show tantalizing evidence for a rapid evolution of the rest-frame ultraviolet (UV) galaxy luminosity function (LF) from $z = 6$ to $z = 8$ and a declining star-formation rate with increasing redshift (Bouwens et al. 2011a,b), as expected on the basis of dark matter halo assembly (Trenti et al. 2010).

However, because the ultradeep datasets cover only a few WFC3/IR fields, their dynamic range is limited by the small volume that they probe. In particular they provide poor constraints on the population of bright galaxies at $z \sim 8$, which are very rare and highly clustered (Trenti et al. 2012b). A complete understanding of the number density and overall shape of the LF at $z \sim 8$ requires a large-area survey to search for the brightest galaxies at these epochs.

Identifying the brightest $z \sim 8$ candidates from broadband photometry is also of fundamental importance to provide the best targets for spectroscopic follow-up studies aimed both at confirming the redshift of the sources as well as inferring the properties of the intergalactic medium (IGM) in proximity of these galaxies (e.g., Schenker et al. 2012; Treu et al. 2012). Spectroscopic

* Based on observations made with the NASA/ESA *Hubble Space Telescope*, obtained at the Space Telescope Science Institute, which is operated by the Association of Universities for Research in Astronomy under NASA contract NAS5-26555. These observations are associated with programs 11519, 11520, 11524, 11528, 11530, 11533, 11534, 11541, 11700, 11702, 12024, 12025, and 12572.

¹ Space Telescope Science Institute, 3700 San Martin Drive Baltimore MD 21218 USA

² Institute of Astronomy, University of Cambridge, Madingley Road, Cambridge, CB3 0HA, United Kingdom

³ Kavli Institute for Cosmology, University of Cambridge, Madingley Road, Cambridge, CB3 0HA, United Kingdom

⁴ UCO/Lick Observatory, University of California, Santa Cruz, CA 95064 USA

⁵ Department of Physics, University of California, Santa Barbara, CA 93106-9530, USA

⁶ Leiden Observatory, Leiden University, NL-2300 RA Leiden, The Netherlands

⁷ CASA, Department of Astrophysical and Planetary Sciences, University of Colorado, 389-UCB, Boulder, CO 80309 USA

⁸ European Space Agency (ESTEC), Keplerlaan 1, 2200 AG, Noordwijk, The Netherlands

[†] Kavli Fellow

[‡] Hubble Fellow

confirmation of the redshift of LBG galaxies has been carried out for large samples at $z \sim 4 - 6$ (e.g., Malhotra et al. 2005; Stark et al. 2011), and recently extended out to $z = 7.2$ (Ono et al. 2012). These studies show that photometrically selected samples of LBGs have very low contamination ($\sim 10\%$, see Malhotra et al. 2005). It is necessary to extend the frontier of spectroscopy further into the epoch of reionization, at $z \sim 8$, not only to provide definitive proof that the LBG selection continues to be reliable for candidates into the reionization epoch, but more importantly to infer the ionization state of the IGM from the study of the Ly α equivalent width distribution of LBG sources (e.g., Treu et al. 2012).

At present there are several ongoing WFC3/IR surveys designed to identify a relatively large sample of bright ($m_{AB} \lesssim 27$; $M_{AB} \lesssim -20$) $z \sim 8$ galaxies, namely the CANDELS Multi-Cycle Treasury (MCT) program (Grogin et al. 2011; Koekemoer et al. 2011), the Hubble Infrared Pure Parallel Imaging Extragalactic Survey (HIPPIES) (Yan et al. 2011b), and the Brightest of Reionizing Galaxies (BoRG) (Trenti et al. 2011, 2012b). In the near term, the sample size of bright $z \gtrsim 7$ galaxies will also be augmented by cluster lensing surveys (e.g., Hall et al. 2012; Bradley et al. 2012), including the Cluster Lensing And Supernova survey with Hubble (CLASH; Postman et al. 2012) MCT program, which recently reported the discovery of a magnified LBG candidate at $z \sim 9.6$ (Zheng et al. 2012). All of these programs take advantage of multi-band *HST* optical NIR data to search for $z \sim 8$ galaxies as Y_{098} or Y_{105} dropouts using the Lyman-break technique (Steidel et al. 1996).

Currently, the shape of the bright-end of the galaxy UV LF at $z = 8$ is debated. Theoretical and numerical investigations predict that it should remain Schechter-like (Schechter 1976), of the form $\phi(L) = \phi_*(L/L_*)^\alpha e^{-(L/L_*)}$, at $z \sim 7 - 10$ (Trenti et al. 2010; Jaacks et al. 2012). Conversely, some numerical studies have suggested a possible excess of sources at the bright end, with a non-Schechter behavior tied to the inefficient onset of AGN feedback at early times (e.g., Finlator et al. 2011).

Observationally, two recent papers from the CANDELS dataset in GOODS-South yielded different results. Yan et al. (2011a) found a significant excess of bright $z \sim 8$ candidates with $M_{AB} < -21.0$ over the expectation from a Schechter function using data from ~ 80 arcmin² of area in the GOODS-South field. The shape of their $z \sim 8$ luminosity function resembles a step function (see their Figure 4). On the other hand, Oesch et al. (2012) analyzed the same dataset and derive a well-behaved Schechter function for bright $z \sim 8$ sources, consistent with the extrapolation of the LF evolution from $z \sim 7$ and with the predictions of the LF model of Trenti et al. (2010). The Oesch et al. (2012) result ($M_{z=8}^* = -19.8^{+0.46}_{-0.57}$) is also consistent with the first-epoch BoRG (BoRG09) determination of the knee of the Schechter function ($M_{z=8}^* = -20.2 \pm 0.3$, with the error bar at a fixed α and ϕ_*). Our initial BoRG data were about 0.5 mag shallower than the current CANDELS dataset, but we already had larger sky coverage (~ 140 arcmin² vs. ~ 80 arcmin²).

Here we take advantage of the additional fields recently acquired as part of the BoRG survey and update the

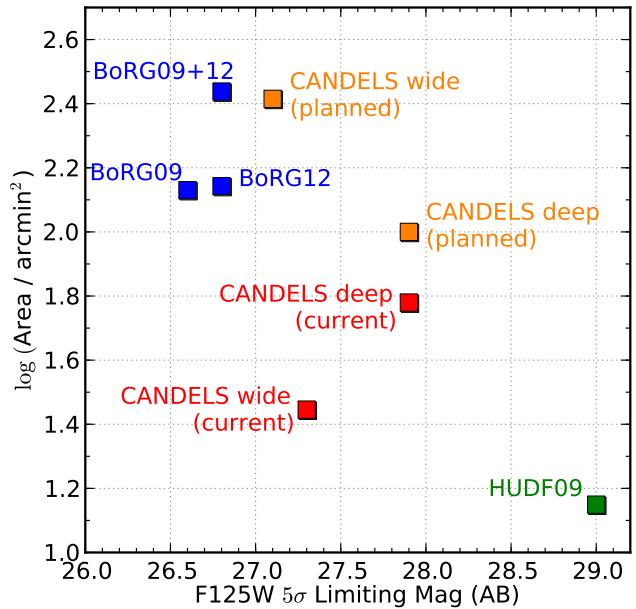


Figure 1. Comparison of area and depth of current surveys that can search for $z \sim 8$ LBGs. Because only ~ 260 arcmin² of the planned CANDELS wide survey includes Y-band imaging (red and orange), the ongoing BoRG survey (blue; ~ 274 arcmin²) provides the largest area for a Y-band dropout survey. The depth of our BoRG survey is only ~ 0.3 mag shallower than the wide part of the CANDELS survey. The ultra-deep HUDF09 WFC3/IR observations are illustrated by the green point.

sample of Y_{098} dropouts described in Trenti et al. (2011, 2012b) to include an additional 139 arcmin² of area. Our latest catalog now contains eight very bright ($> 8\sigma$) $z \sim 8$ candidates and an additional 25 bright $z \sim 8$ candidates detected at lower significance ($> 5\sigma$), with $M \sim M_{z=8}^*$. This is currently the largest-area search for $z \sim 8$ candidates, now totaling ~ 274 arcmin². Additionally, given the random pointing nature of our pure-parallel *HST* program, the BoRG dataset is distinct in that it is minimally affected by cosmic variance (Trenti & Stiavelli 2008). Therefore, this catalog is uniquely positioned to set the tightest constraints on the number density of the brightest $z \sim 8$ galaxies and the bright end of the rest-frame ultraviolet galaxy luminosity function ($M_{UV} \leq -19.6$; $L \geq 0.5L_{z=8}^*$).

This paper is organized as follows. We describe the BoRG survey in Section 2. We present the observations and photometry in Section 3 and dropout selection in Section 4. The results and constraints on the $z \sim 8$ UV LF are discussed in Section 5. We summarize our results and conclusions in Section 6. Throughout this work, we assume a cosmology with $\Omega_m = 0.3$, $\Omega_\Lambda = 0.7$, and $H_0 = 70$ km s⁻¹ Mpc⁻¹. This provides an angular scale of 4.8 (proper) kpc arcsec⁻¹ at $z = 8.0$. All magnitudes are expressed in the AB photometric system (Oke 1974).

2. THE BORG SURVEY FOR $z \sim 8$ GALAXIES

In 2009 we initiated the BoRG survey, a pure-parallel WFC3 survey that complements deep and ultra-deep WFC3/IR observations by looking for very bright ($m_{AB} \lesssim 27$; $M_{AB} \lesssim -20$) galaxies at $z \gtrsim 7.5$ (Trenti et al. 2011, 2012b) by obtaining WFC3 imaging in four filters (F606W, F098M, F125W, F160W) on random

Table 1
BoRG09 Survey Fields, Exposure Times, and 5σ Limiting Magnitudes^a

Field	Alternate Name ^b	PID	α_{J2000} (deg)	δ_{J2000} (deg)	F600LP		F606W		F098M		F125W		F160W	
					t (s)	m_{lim}	t (s)	m_{lim}	t (s)	m_{lim}	t (s)	m_{lim}	t (s)	m_{lim}
borg_0214+1255	yan24	11702	33.410	12.915	2294	25.9			2806	25.9	1403	25.9	1403	25.7
borg_0540-6409	borg2n	11700	84.879	-64.151			3171	26.9	4112	26.6	2309	26.6	1406	26.3
borg_0553-6405	borg81	11700	88.276	-64.088			3624	27.0	6418	27.0	2612	26.8	2012	26.3
borg_0624-6432	borg2t ^d	11700	95.898	-64.528			2133	26.7	1806	26.3	1206	26.4	503	25.6
borg_0624-6440	borg2k	11700	95.951	-64.663			2135	26.7	2909	26.6	1206	26.6	906	26.0
borg_0637-7518 ^c	borg93	11700	99.265	-75.313			4290	26.7	6218	26.7	2412	26.6	1612	26.0
borg_0751+2917	borg0t	11700 ^e	117.709	29.282	3732	26.6	2826	26.8	18641	27.4	5115	27.1	3912	26.8
borg_0756+3043	borg0c	11700	118.989	30.718			2600	26.7	4712	26.7	1906	26.6	1406	26.2
borg_0808+3946	borg1n	11700	122.089	39.759			2600	26.5	4612	26.4	2206	26.6	1406	26.0
borg_0819+4911	borg0g	11700	124.830	49.184			1908	26.4	3009	26.6	1206	26.5	806	25.8
borg_0820+2332	borg30 ^d	11700	125.014	23.535			2556	26.7	3109	26.5	703	26.1	703	25.8
borg_0906+0255	borg73	11700	136.405	2.925			3106	26.9	5518	27.0	2709	27.0	1906	26.6
borg_0909+0002	borg66	11700	137.286	-0.030			2650	26.8	3909	26.8	1806	26.7	1006	26.0
borg_0914+2822	borg39	11700	138.569	28.362			2571	26.8	4615	26.8	2206	26.8	1706	26.5
borg_0922+4505	borg1r	11700	140.406	45.088			2708	26.6	4812	26.6	2106	26.5	1706	26.3
borg_0926+4000	borg45	11700	141.393	40.006			1276	26.2	2806	26.3	1106	26.2	903	25.9
borg_0926+4426	yan28	11702	141.382	44.426	2374	26.6			6012	27.1	1603	26.7	1403	26.5
borg_1031+3804	borg70	11700	157.715	38.059			1815	26.4	3109	26.4	1506	26.3	1306	26.0
borg_1152+5441	borg0y	11700	177.958	54.684			2898	27.0	6021	27.0	2809	27.1	1906	26.7
borg_1153+0056	borg0j	11700	178.182	0.931			2647	26.8	4515	26.7	2209	26.7	1606	26.4
borg_1209+4543	borg0p	11700 ^e	182.355	45.724	2234	26.6	2707	27.0	13729	27.4	3709	27.2	2909	26.8
borg_1230+0750	borg1v	11700	187.470	7.825			2436	26.6	4112	26.1	1806	26.0	1406	25.6
borg_1242+5716	yan11	11702	190.554	57.270	2800	26.5			5215	27.0	2509	26.9	2309	26.6
borg_1245+3356	borg49	11700	191.186	33.936			1789	26.7	3409	26.8	1506	26.7	1106	26.2
borg_1337+0028	yan19	11702	204.202	-0.464	2270	26.4			6818	27.0	1203	26.6	1203	26.3
borg_1341+4123	yan32	11702	205.131	41.384	3810	27.0			17435	27.6	3206	27.2	2806	26.9
borg_1437+5043	borg58	11700	219.234	50.719			2754	26.9	4912	27.0	2509	27.0	1806	26.5
borg_1524+0954	yan51	11702	231.041	9.906	2078	26.3			8718	27.0	1603	26.5	1303	26.2
borg_1632+3737	borg1k	11700	247.892	37.609			1260	26.4	2909	26.7	1206	26.6	906	26.0

Note. — The total survey area of BoRG09 is ~ 135 arcmin², with an effective search area for Y_{098} dropouts of ~ 98 arcmin² after accounting for incompleteness. Unless otherwise noted, each field has an area of 4.7 arcmin².

^a 5σ magnitude limits in a $r = 0.32'$ aperture, corrected for Galactic extinction.

^b Used in Trenti et al. (2011).

^c Field has multiple, partially overlapping exposures for a total area 6.9 arcmin². Exposure times quoted are the sum of all exposures.

^d Data missing due to scheduling constraint/conflict.

^e Also includes data from HIPPIES program 11702.

sightlines at high Galactic latitudes ($|b| > 30^\circ$). Because luminous massive galaxies at these redshifts are expected to be clustered (Trenti et al. 2012b), the random pointing nature of our BoRG survey is ideal to mitigate the severe effects of cosmic variance (Trenti & Stiavelli 2008; Robertson 2010). In fact, our current survey geometry of 59 independent WFC3/IR fields makes our number counts of $z \sim 8$ galaxies essentially follow a Poisson distribution and can be used to constrain the luminosity function as well as a contiguous single-field survey with about two times more area at the same depth. If all the BoRG area had been in a single field of 16.5×16.5 arcmin², we derive from Trenti & Stiavelli (2008) that cosmic variance would have dominated over Poisson uncertainty for a sample of 33 candidates (22% vs. 17% respectively, for a total fractional error of 28%).

By reducing the uncertainty in the number density of bright sources due to cosmic variance, we can place stronger observational constraints on L_* (or M_*), the characteristic luminosity of the LF. This, in turn, can help break the well-known degeneracy between M_* and α , the faint-end slope, when fitting a Schechter (1976) luminosity function to the data. Placing tighter constraints on the value of α at redshifts $z \gtrsim 6$ is crucial in determining the contribution of galaxies to the reionization of the universe. Further, the relative brightness of the LBGs discovered in the BoRG survey can possibly

place $z \sim 8$ galaxies within reach of ground-based spectroscopic follow-up observations, as has been attempted on some of our brighter candidates (Schenker et al. 2012; Treu et al. 2012).

Our ongoing BoRG survey has covered 274 arcmin² to date thanks both to its continuation in Cycle 19 (GO 12752, PI Trenti) and by assimilating data from the similar HIPPIES pure-parallel program (Yan et al. 2011b) as well as the coordinated parallel observations acquired as part of the Cosmic Origins Spectrograph (COS) GTO program. As illustrated in Figure 1, the BoRG survey is ~ 0.3 mag shallower than the “wide” part of the CANDELS program that has Y_{105} -band data, but has a larger area with Y_{098} (or Y_{105}), J_{125} , and H_{160} band coverage that is needed to search for $z \sim 8$ galaxies.

In this paper we focus on $z \sim 8$ LBG candidates selected as Y_{098} -band dropouts. To use a homogeneous selection of $z \sim 8$ candidates, we specifically exclude the HIPPIES Cycle 18 dataset, which replaced the F098M band with the F105W band. We leave the identification of $z \sim 8$ Y_{105} -band dropouts for discussion in a future paper.

3. OBSERVATIONS AND PHOTOMETRY

The primary goal of the BoRG survey is to identify galaxies at $z \sim 8$ and measure the bright end of the LBG rest-frame ultraviolet LF at this redshift. Our

Table 2
BoRG12 Survey Fields, Exposure Times, and 5σ Limiting Magnitudes^a

Field	PID	α_{J2000} (deg)	δ_{J2000} (deg)	F600LP		F606W		F098M		F125W		F160W	
				t (s)	m_{lim}	t (s)	m_{lim}	t (s)	m_{lim}	t (s)	m_{lim}	t (s)	m_{lim}
borg_0110-0224 ^b	11700 ^d	17.532	-2.395	3892	26.7	13911	26.9	39297	27.0	13538	26.9	10032	26.6
borg_0228-4102	11541	36.987	-41.026	1414	26.5			3406	26.9	1403	26.8	1403	26.5
borg_0240-1857	11541	40.114	-18.954	1360	26.4			3406	26.8	1403	26.7	1403	26.5
borg_0427+2538	11533	66.690	25.640	1200	24.1			2409	25.2	703	25.1	503	25.0
borg_0436-5259	11520	69.059	-52.986	1932	26.6			4406	27.1	2906	27.3	2206	26.8
borg_0439-5317	11520	69.855	-53.278	1932	26.6			4206	27.0	3006	27.2	2306	26.8
borg_0440-5244	11520	69.959	-52.731	1932	26.5			6609	27.2	2003	27.0	1403	26.5
borg_0835+2456	12025	128.821	24.936			4698	26.8	4209	26.7	2206	26.7	2009	26.3
borg_0846+7654	11520	131.593	76.893	1401	26.4			4406	27.0	2003	27.1	1603	26.6
borg_1010+3001	12025	152.406	30.018			9142	27.2	5612	26.8	3212	26.8	2812	26.6
borg_1014-0423	11524	153.523	-4.379	1221	26.3			1909	25.6	1106	26.2	703	25.9
borg_1031+5052 ^c	12025	157.691	50.862			9991	27.4	9629	26.9	4812	27.1	4212	26.8
borg_1033+5051 ^c	12025	158.212	50.860			9640	27.3	6412	26.8	3212	26.8	2812	26.5
borg_1051+3359	12024	162.822	33.985			4220	26.9	6235	26.8	3318	27.0	1912	26.4
borg_1103-2330	12025	165.808	-23.506			8558	27.0	9429	27.1	4412	27.2	3612	26.8
borg_1111+5545	12025	167.737	55.751			6524	27.1	5518	26.9	2606	27.0	2409	26.6
borg_1119+4026	11519	169.514	40.398	1308	26.2			2206	26.6	1403	26.8	1403	26.4
borg_1131+3114	11519	172.876	31.289	1316	26.5			2106	26.5	1403	26.8	1403	26.4
borg_1301+0000	11702	195.318	-0.007	2150	26.1			5812	26.4	1603	26.1	1303	25.9
borg_1408+5503	12572	211.993	55.056			3324	26.9	5623	26.9	2612	26.9	2612	26.6
borg_1510+1115	12572	227.537	11.242			5326	26.9	8423	27.1	3812	27.1	3812	26.8
borg_1555+1108	12025	238.857	11.132			4753	26.9	5515	27.0	2909	27.0	2509	26.7
borg_1632+3733	11700	248.074	37.557			2751	26.8	5115	26.9	2406	27.0	1806	26.5
borg_1815-3244	11533	273.628	-32.734	1200	22.3			2509	21.8	703	21.6	403	21.5
borg_2057-4412	11530	314.340	-44.207	2500	26.4			5009	26.7	1203	26.4	803	25.9
borg_2132+1004	11524	323.062	10.064	1355	26.2			2409	26.5	1006	26.4	503	25.7
borg_2155-4411	11541	328.812	-44.177	2130	26.7			5609	27.0	1403	26.7	903	26.2
borg_2203+1851	11534	330.705	18.850	3200	26.8			17229	27.4	2006	26.8	2806	26.8
borg_2345+0054	11702	356.261	-0.902	2028	26.4			5612	27.0	1403	26.8	1403	26.5
borg_2351-4332	11528	357.650	-43.525	1050	26.3			11123	27.4	4209	27.3	2806	26.7

Note. — The total survey area of BoRG12 is ~ 139 arcmin², with an effective search area for Y_{098} dropouts of ~ 115 arcmin² after accounting for incompleteness. The combined survey area of BoRG09+BoRG12 is ~ 274 arcmin², with an effective search area for Y_{098} dropouts of ~ 213 arcmin². Unless otherwise noted, each field has an area of 4.7 arcmin².

^a 5σ magnitude limits in a $r = 0.32'$ aperture, corrected for Galactic extinction.

^b Field has multiple, partially overlapping exposures for a total area 14.8 arcmin². Exposure times quoted are the sum of all exposures.

^c Field has multiple, partially overlapping exposures for a total area 5.9 arcmin². Exposure times quoted are the sum of all exposures.

^d Also includes data from HIPPIES program 11702.

Table 3
Photometry of Y_{098} -dropout ($z \sim 8$) Candidates in the 8σ Catalog

ID	α_{J2000}	δ_{J2000}	J_{125} ^a	$Y_{098} - J_{125}$	$J_{125} - H_{160}$	S/N_V ^b	S/N_{098}	S/N_{125}	S/N_{160}
borg_0440-5244_682	69.9455843	-52.7320162	25.9 ± 0.1	> 2.1	0.0 ± 0.3	-0.8	-0.5	9.1	5.7
borg_0751+2917_229	117.7141714	29.2715323	26.5 ± 0.2	> 2.5	-0.0 ± 0.3	-0.9	0.0	8.9	6.5
borg_0909+0002_595	137.2731625	-0.0297391	26.1 ± 0.2	1.8 ± 0.6	-0.4 ± 0.4	-0.5	1.8	8.6	3.2
borg_1033+5051_126	158.1863098	50.8416866	26.0 ± 0.2	> 2.5	-0.2 ± 0.3	0.0	-0.6	8.1	5.6
borg_1301+0000_160	195.3070838	-0.0189297	25.5 ± 0.2	2.1 ± 0.6	-0.4 ± 0.3	0.7	1.7	9.5	5.2
borg_1437+5043_1137	219.210672	50.7260085	26.1 ± 0.1	> 2.7	0.0 ± 0.2	-1.5	-1.0	10.9	7.9
borg_1555+1108_1417	238.8651549	11.1393576	26.6 ± 0.2	1.9 ± 0.7	-0.6 ± 0.4	1.1	1.4	8.4	3.4
borg_2203+1851_1061	330.6930404	18.8581986	26.0 ± 0.2	2.5 ± 0.6	-0.3 ± 0.3	0.2	1.6	9.4	6.6

^a Total magnitudes (AUTOMAG).

^b V_{606} whenever possible; otherwise V_{600LP} .

observations are designed to acquire WFC3 imaging in four filters (F606W, F098M, F125W, F160W), which are obtained on random and discrete sightlines inherent to this being a pure-parallel program. We identify bright ($J_{125} \lesssim 27$) high-redshift galaxies by searching for Y_{098} dropouts using the well-known Lyman-break dropout technique (Steidel et al. 1996). The J_{125} and H_{160} bands are used for source detection and to measure the rest-frame UV color, while the WFC3/UVIS V_{606} band is used to reject low-redshift ($z \sim 1.5 - 2$) interloper galax-

ies, which are the primary source of contamination to our $z \gtrsim 7.5$ sample. As discussed in Section 4, our BoRG survey is optimized to minimize the probability of contamination from both low-redshift interlopers and cool dwarf stars.

We also included data from the similar HIPPIES WFC3 pure-parallel program Yan et al. (2011b) and the coordinated parallel observations from the COS GTO program. The filter selection of the HIPPIES program and the earlier part of COS GTO program differs from

Table 4
Photometry of Y_{098} -dropout ($z \sim 8$) Candidates in the 5σ Catalog

ID	α_{J2000}	δ_{J2000}	J_{125}^a	$Y_{098} - J_{125}$	$J_{125} - H_{160}$	S/N_V^b	S/N_{098}	S/N_{125}	S/N_{160}
borg_0436-5259_1233	69.0303878	-52.9717897	27.1 ± 0.2	> 1.8	-0.4 ± 0.5	1.4	0.9	5.5	2.6
borg_0553-6405_4006	88.2647181	-64.0821631	26.7 ± 0.2	> 2.3	0.1 ± 0.3	0.2	0.6	6.8	4.7
borg_0751+2917_920	117.706444	29.2977181	27.0 ± 0.2	> 2.3	-0.6 ± 0.4	-0.3	-0.0	7.1	3.3
borg_0756+3043_437	118.9794155	30.7177854	26.5 ± 0.2	> 2.2	-0.0 ± 0.3	1.3	0.9	6.8	4.6
borg_0835+2456_253	128.8067291	24.9267442	26.2 ± 0.2	2.0 ± 0.8	-0.2 ± 0.4	-1.2	1.1	6.8	4.1
borg_1031+3804_213	157.7102797	38.0497128	26.6 ± 0.3	> 1.9	-0.1 ± 0.4	0.3	0.7	5.4	4.0
borg_1031+3804_831	157.7353387	38.0673682	26.6 ± 0.3	> 1.9	-0.5 ± 0.5	1.4	0.3	5.5	2.9
borg_1103-2330_1180	165.7881655	-23.4990798	26.7 ± 0.2	> 2.2	0.0 ± 0.3	-0.3	-0.4	7.8	5.8
borg_1131+3114_1244	172.8573532	31.2942314	26.2 ± 0.2	> 2.0	-0.3 ± 0.3	0.8	-0.2	7.7	4.3
borg_1152+5441_1087	177.9750532	54.6979452	27.2 ± 0.3	> 1.8	-0.2 ± 0.4	1.2	0.9	5.5	3.2
borg_1153+0056_540	178.1909931	0.9320074	27.0 ± 0.3	1.9 ± 0.8	-0.5 ± 0.4	0.2	1.1	5.9	3.2
borg_1242+5716_159	190.5672023	57.2567197	26.4 ± 0.2	> 2.2	-0.2 ± 0.4	0.0	0.4	6.6	4.3
borg_1408+5503_749	212.0126402	55.0585147	26.5 ± 0.2	> 2.0	-0.2 ± 0.3	-1.1	0.8	6.7	4.4
borg_1408+5503_980	212.0082405	55.0672755	27.0 ± 0.2	1.9 ± 0.8	-0.4 ± 0.4	-0.2	1.0	6.0	3.5
borg_1437+5043_172	219.2223469	50.7080907	27.1 ± 0.2	2.0 ± 0.8	-0.4 ± 0.5	1.0	1.0	5.8	2.8
borg_1437+5043_879	219.2240496	50.7259683	27.3 ± 0.3	> 1.8	-0.3 ± 0.5	0.3	0.5	5.0	2.7
borg_1510+1115_51	227.5348783	11.2225448	26.7 ± 0.2	1.9 ± 0.8	-0.2 ± 0.4	1.2	1.0	6.2	3.9
borg_1510+1115_1236	227.5521577	11.2522441	27.2 ± 0.3	> 2.0	-0.4 ± 0.4	1.1	0.7	6.3	3.5
borg_1510+1115_1404	227.5425951	11.2615405	26.7 ± 0.2	> 1.9	-0.3 ± 0.4	0.8	0.7	6.5	4.0
borg_1555+1108_595	238.8429322	11.1279017	27.3 ± 0.3	> 1.9	-0.2 ± 0.4	0.8	-0.1	5.7	3.2
borg_1555+1108_1166	238.8438689	11.1420588	27.2 ± 0.2	> 1.9	-0.3 ± 0.4	1.2	0.2	5.8	2.9
borg_1632+3733_694	248.0628393	37.5568592	27.4 ± 0.3	> 2.0	-0.4 ± 0.5	0.9	0.7	6.2	2.7
borg_2132+1004_24	323.0575947	10.0443562	26.5 ± 0.2	> 2.1	0.0 ± 0.4	1.4	0.6	5.3	3.2
borg_2155-4411_341	328.8301017	-44.1819169	26.6 ± 0.2	> 2.5	-0.4 ± 0.4	0.0	-1.1	7.3	3.4
borg_2155-4411_1192	328.8031162	-44.1737506	26.9 ± 0.3	> 2.1	-0.1 ± 0.5	-0.7	0.6	5.2	3.1

Note. — Sources reported in the 8σ catalog (Table 3) are not duplicated here, but of course are included in the 5σ catalog.

^a Total magnitudes (AUTOMAG).

^b V_{606} whenever possible; otherwise V_{600LP} .

Table 5
New Photometry of Y_{098} -dropout ($z \sim 8$) Candidates in the BoRG58 Protocluster (Trenti et al. 2012b)

ID	α_{J2000}	δ_{J2000}	J_{125}^a	$Y_{098} - J_{125}$	$J_{125} - H_{160}$	S/N_{606}	S/N_{098}	S/N_{125}	S/N_{160}
borg_1437+5043_1137	219.210672	50.7260085	26.1 ± 0.1	> 2.7	0.0 ± 0.2	-1.5	-1.0	10.9	7.9
borg_1437+5043_879	219.2240496	50.7259683	27.3 ± 0.3	> 1.8	-0.3 ± 0.5	0.3	0.5	5.0	2.7
borg_1437+5043_757	219.2310489	50.7240585	27.1 ± 0.2	> 1.8	-0.7 ± 0.6	1.1	-0.5	5.0	1.7
borg_1437+5043_435	219.2202746	50.7156344	27.4 ± 0.3	> 1.8	0.0 ± 0.4	0.6	0.6	4.9	3.3
borg_1437+5043_172	219.2223469	50.7080907	27.1 ± 0.2	2.0 ± 0.8	-0.4 ± 0.5	1.0	1.0	5.8	2.8

^a Total magnitudes (AUTOMAG).

Table 6
Photometry of Other Possible Y_{098} -dropout ($z \sim 8$) Candidates

ID	α_{J2000}	δ_{J2000}	J_{125}^a	$Y_{098} - J_{125}$	$J_{125} - H_{160}$	S/N_V^b	S/N_{098}	S/N_{125}	S/N_{160}
borg_0240-1857_392 ^c	40.0998766	-18.9604896	26.2 ± 0.2	2.1 ± 0.7	-0.1 ± 0.3	0.6	1.4	8.1	6.3
borg_1632+3737_386 ^d	247.8986483	37.6047539	25.1 ± 0.1	1.9 ± 0.4	0.0 ± 0.2	-0.0	3.1	14.2	9.3

^a Total magnitudes (AUTOMAG).

^b V_{606} whenever possible; otherwise V_{600LP} .

^c Unresolved source; possible QSO candidate or most likely an L/T dwarf star with an unusually red $Y_{098} - J_{125}$ color.

^d Photometry contaminated by an adjacent bright source with similar colors ($Y_{098} - J_{125} = 1.6$), but clearly detected in V_{606} and Y_{098} ; most likely a low-redshift contaminant.

BoRG in that those datasets used the F600LP filter instead of F606W to control for contamination from reddened low-redshift sources. Trenti et al. (2011) discuss the benefits of F606W compared to F600LP. Here we reiterate that, because F606W has a larger transmission efficiency integrated in frequency space over the pass-band, it reaches deeper at fixed integration time. This also becomes apparent in the data, for example in field borg_0751 + 2917 (Table 1), which has deeper data in F606W ($m_{lim} = 26.8$ with $t = 2826$ s) compared to

F600LP ($m_{lim} = 26.6$ with $t = 3732$ s) despite the shorter integration time.

Pure-parallel observations come with a unique set of challenges. Because the primary observations are spectroscopic in nature, dithering is mostly absent in our pure-parallel WFC3 data. As a result, detector artifacts (e.g., hot/warm pixels), uncorrected cosmic rays, and WFC3/IR detector persistence must be carefully considered in the data reduction and data analysis. To mitigate detector hot/warm pixels and cosmic rays, we employed

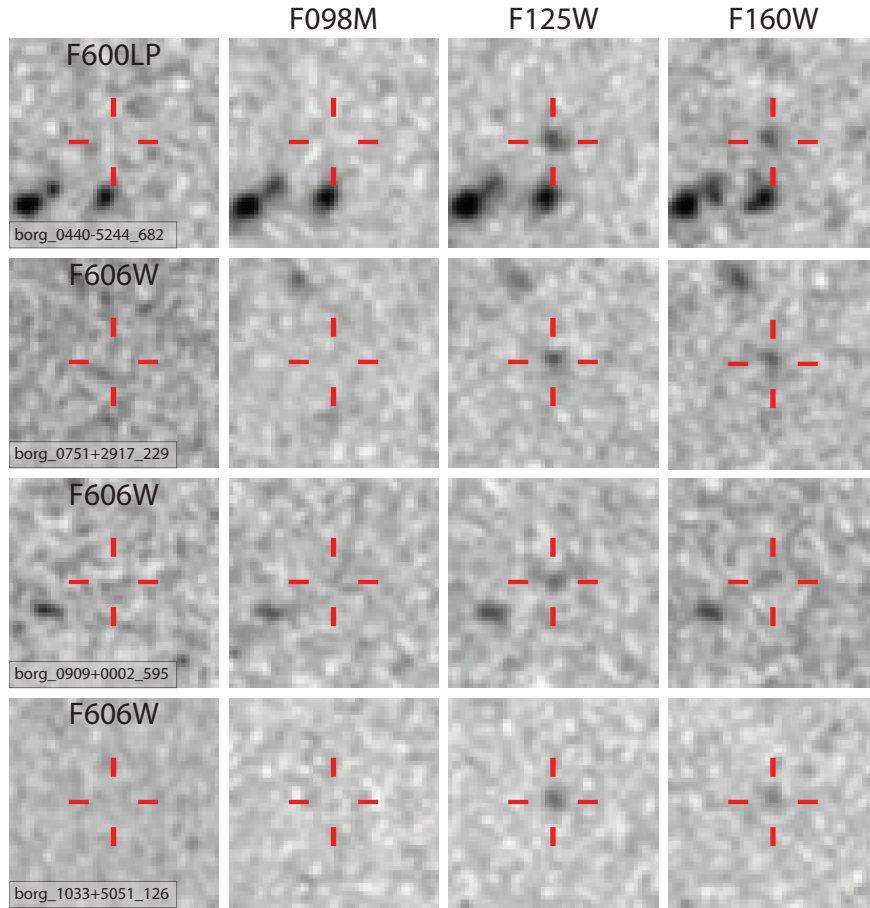


Figure 2. Postage-stamp cutout images of four of the very bright ($\gtrsim 8\sigma$) high-redshift Y_{098} -dropout candidate galaxies. The cutout images are $4' \times 4'$, corresponding to 19.2 kpc on a side at $z = 8$, and are shown with a P.A. = 0° .

a robust algorithm based on a variation of Laplacian edge detection (van Dokkum 2001) to filter the individual FLT files prior to combining them with `MultiDrizzle` (Koekemoer et al. 2002). The parameters for the algorithm were chosen to remove most sharp-edged artifacts from the data, but to also be rather conservative so as not to remove any real sources.

As detailed in Trenti et al. (2011), our observing strategy is also unique because it is designed to minimize the impact of WFC3/IR detector persistence from observations taken in orbits immediately prior to our exposures. We take advantage of the property that the amount of residual image persistence appears to decay roughly as a power law with time. Briefly, observations in either the J_{125} band or H_{160} band are preceded in the same orbit by a comparably long Y_{098} band exposure, and whenever possible, J_{125} -band exposures precede those in H_{160} band¹². Therefore any persistent residual images from prior observations will be brighter in the bluer bands and thus will not contaminate our high-redshift dropout sample.

`MultiDrizzle` (Koekemoer et al. 2002) was used to combine individual exposures in a given filter to produce the final science images as well as the associated inverse-variance weight maps. The images are drizzled

to a final pixel scale of $0.08''/\text{pixel}$. Because BoRG is a pure-parallel program, the image depths vary among our fields. For a typical 4-orbit parallel field, we obtain exposures of 2200 s, 3800 s, 1800 s, and 1800 s in V_{606} , Y_{098} , J_{125} , and H_{160} , respectively. In a $0.4''$ diameter aperture, the corresponding 5σ limiting magnitudes are approximately 27.4, 27.1, 26.9, and 26.6, respectively. In Table 1, we list the survey fields, exposure times, and 5σ limiting magnitudes ($r = 0.32''$ aperture) of the initial BoRG09 dataset (Trenti et al. 2011), and in Table 2 we list the same properties for the new fields in the significantly expanded BoRG12 dataset. We have released the reduced drizzled science and RMS images for the BoRG dataset, which is publicly available via the BoRG website at wolf359.colorado.edu and the High Level Science Products on the MAST website¹³.

We used `SExtractor` (Bertin & Arnouts 1996) in dual-image mode for object detection and photometry. For the detection image we used the WFC3/IR J_{125} data. The inverse-variance weight images produced by `MultiDrizzle` were used to generate RMS maps for each image. We subsequently normalized the RMS maps to account for correlated noise introduced by the drizzling procedure (see Trenti et al. 2011) and used them in `SExtractor` for both source detection and photometry. Sources were required to have at least 9 contiguous pixels, each detected at a threshold of 0.7σ above the back-

¹² This Phase II strategy is implemented in GO 11700 and GO 12752 (PI: Trenti), as well as the more recent COS-GTO parallel observations.

¹³ archive.stsci.edu/prepds/borg

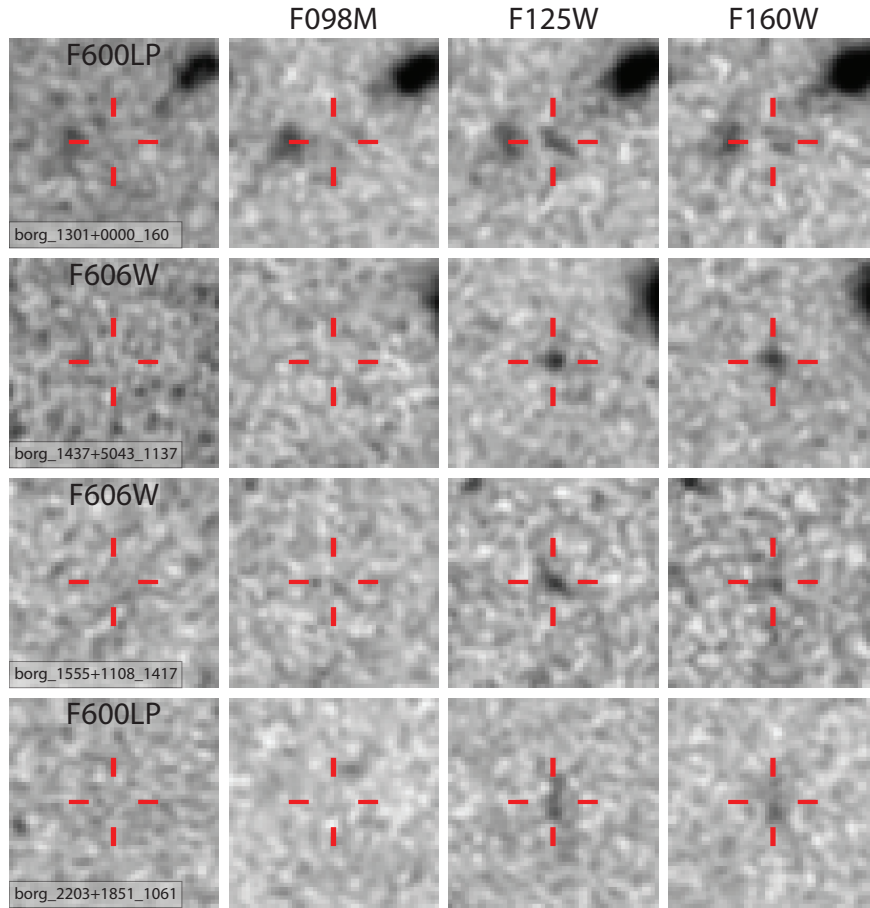


Figure 3. Postage-stamp cutout images of four of the very bright ($\gtrsim 8\sigma$) high-redshift Y_{098} -dropout candidate galaxies. The cutout images are $4' \times 4'$, corresponding to 19.2 kpc on a side at $z = 8$, and are shown with a P.A. = 0° .

ground. Object colors and signal-to-noise values were measured using isophotal magnitudes (ISOMAG) and total magnitudes were measured within scalable Kron apertures (AUTOMAG).

The photometry in each field has been corrected for Galactic extinction using the Schlegel et al. (1998) dust maps. All measurements given in this paper include this correction, which is typically modest $A_V \lesssim 0.2$ because the survey primarily targets lines of sight at high galactic latitudes.

4. SELECTION OF $z \sim 8$ Y_{098} -BAND DROPOUT CANDIDATES

We searched for $z \gtrsim 7.5$ galaxies using a Y_{098} -dropout selection criteria in two broadband colors. The general criteria are a strong break between the Y_{098} and J_{125} filters, a relatively blue or flat $J_{125} - H_{160}$ color, and a non-detection in the optical V_{606} (or V_{600LP}) band. Specifically, following Trenti et al. (2011, 2012b) we require:

$$\begin{aligned} S/N_{Vband} &< 1.5 \\ (Y_{098} - J_{125}) &> 1.75 \\ (J_{125} - H_{160}) &< 0.02 + 0.15[(Y_{098} - J_{125}) - 1.75]. \end{aligned}$$

These criteria select galaxies with redshifts in the range $z \sim 7.4 - 8.8$ (see Section 5). To minimize the probability

of contamination of our sample by low-redshift interlopers, we impose a conservative non-detection threshold of 1.5σ on the optical-band data. The non-detection in the optical V band is fundamental to produce a clean sample of $z \sim 8$ candidates (see Bouwens et al. 2011b). If a source is not detected in a given filter, we set its magnitude to the corresponding 1σ upper limit to calculate its colors. For our final catalog, we require sources to be detected with a signal-to-noise (S/N) threshold of $S/N \geq 5$ in J_{125} and $S/N \geq 2.5$ in H_{160} , as measured in isophotal apertures (ISOMAG). For the bright 8σ catalog, we require sources to be detected with a signal-to-noise threshold of $S/N \geq 8$ in J_{125} and $S/N \geq 3.0$ in H_{160} .

Using these color criteria, we identified 33 relatively bright Y_{098} -dropout galaxy candidates with observed J_{125} band magnitudes between 25.5 and 27.4 mag over our 274 arcmin² search area. Eight of these $z \sim 8$ LBG candidates are brighter than 26.6 mag and are detected at a significance level of $> 8\sigma$ in J_{125} . This is the largest sample of bright ($J_{125} \lesssim 27.4$) $z \sim 8$ galaxies presented to date. We list the properties of the candidates in the 8σ and 5σ catalogs in Tables 3 and 4, respectively. The postage-stamp cutout images of the eight 8σ candidates are shown in Figures 2 and 3.

The $(Y_{098} - J_{125})$ and $(J_{125} - H_{160})$ colors of our $z \sim 8$ candidates along with the color-color selection criteria are illustrated in Figure 4. We also show the expected colors of galaxies simulated over a wide range of redshifts

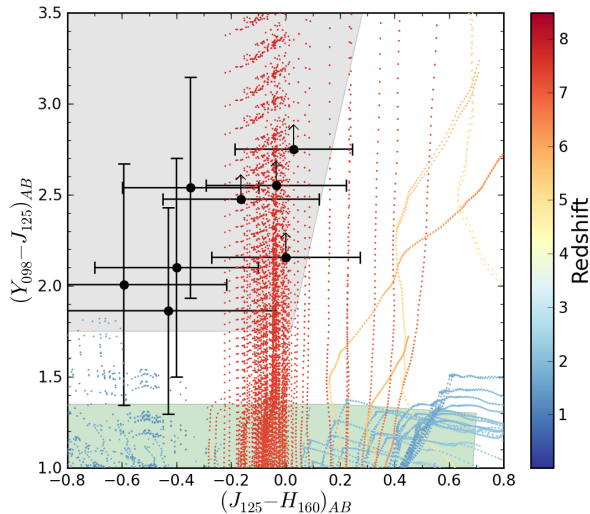


Figure 4. $Y_{098} - J_{125}$ vs. $J_{125} - H_{160}$ two-color diagram used to select our Y_{098} -band dropout candidates. The colors of our 8σ sources are shown by the black data points. The error bars and lower limits are 1σ (68% confidence). The gray region represents the $Y_{098} - J_{125}$ and $J_{125} - H_{160}$ colors of our selection criteria. The colored points represent the expected colors of galaxies simulated over a wide range in redshifts. The green region indicates the colors of low-mass L,T dwarf stars (e.g., Knapp et al. 2004; Ryan et al. 2011; Holwerda et al. 2012 (in prep)). In addition to the color-color selection shown here, Y_{098} -dropouts also need to be undetected ($S/N < 1.5$) in the deep optical imaging performed in the V band by the BoRG survey. The non-detection in V band is fundamental to produce a clean sample of $z \sim 8$ candidates (see Bouwens et al. 2011b).

and also those of low-mass dwarf stars (e.g., Knapp et al. 2004; Ryan et al. 2011; Holwerda et al. 2012 (in prep)). As Figure 4 shows, our conservative $Y_{098} - J_{125} > 1.75$ color criterion is effective in minimizing contamination from cool dwarf stars and low-redshift interlopers.

4.1. Comparison with the Earlier BoRG09 Sample

In this paper we employ an improved data reduction that includes Laplacian filtering (see Section 3). Therefore, we expect some photometric scatter within the measurement uncertainty with respect to the previous catalogs of Y_{098} dropouts published in Trenti et al. (2011, 2012b). Indeed, this is the case: one of the four bright dropouts identified in Trenti et al. (2011), source “BoRG1k”, is now just marginally out of the catalog with $Y_{098} - J_{125} = 1.70$. This is not surprising, as that candidate was at the edge of the selection window in the previous photometry and we were already considering it likely ($p \sim 60\%$) to be a contaminant that scattered into the dropout selection (see Section 5.2 in Trenti et al. 2011). While it was, and still is, uncertain whether this source is at $z \sim 8$, our artificial source recovery simulations (see Section 5) take photometric scatter into account when determining the effective volume of the survey, making the derivation of the luminosity function robust.

With the new data reduction we also verified the photometry for field BoRG58 (here borg_1437+5043), where we identified a $z \sim 8$ protocluster candidate Trenti et al. (2012b). The improved photometry confirms the previous measurements, although we note that two of the fainter $z \sim 8$ candidates have scattered out of our current catalog. In this new reduction and catalog, they are

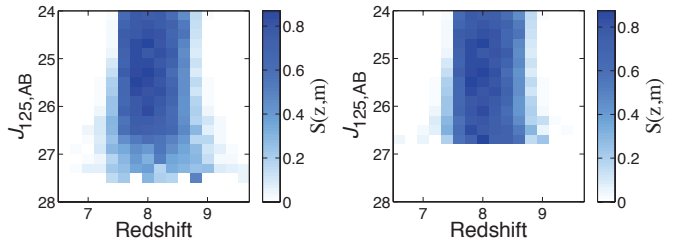


Figure 5. The $S(z, m)$ magnitude-dependent redshift selection function of one representative BoRG survey field, borg_1437+5043, for both the 5σ (left) and 8σ (right) $z \sim 8$ source catalogs. These selection functions were obtained through simulations to recover artificial sources in the BoRG images, as discussed in Section 5. Through these simulations, we computed $S(z, m)$ for each of the 59 individual BoRG fields. detected in the J_{125} band at 4.98σ and 4.88σ , slightly below our formal threshold of 5σ detections (see Table 5). It is worth noting that two new Y_{098} -dropout sources are also detected in this field, just below the detection threshold, at $S/N \sim 4.5$ in J_{125} , providing circumstantial evidence that the overdensity extends to fainter luminosities in line with our theoretical and numerical predictions (Trenti et al. 2012b). Deeper *HST* imaging would be very useful to further investigate the nature of this overdensity.

4.2. Possible $z \sim 8$ Candidates Excluded from the Strict Sample

While two additional candidates pass our 8σ selection criteria (see Table 6), we exclude them from our final catalog. One of these sources (borg_0240-1857_392) is extremely compact and clearly unresolved. Given its compactness, the likely explanation is that source is a Galactic star with either a significant fluctuation in the photometric measurement or with an unusually red $Y_{098} - J_{125}$ intrinsic color (at the $\sim 2\sigma$ level). Because this object is located right above the Galactic Center ($l = 354.36830034^\circ$, $b = 23.48948421^\circ$), the source is most likely a reddened L or T dwarf star. An exciting, but much less likely, alternative would be a $z \sim 8$ QSO, although the limited area of BoRG implies that this occurs with $p \lesssim 5\%$ based on the Willott et al. (2010) QSO luminosity function predictions.

The other source we excluded (borg_1632+3737_386) is extremely bright at 25.1 AB mag in the J_{125} band and located immediately adjacent (SExtractor extraction flag “2”) to an even brighter ($J_{125} = 21.4$ mag) foreground spiral galaxy. The spiral galaxy is tidally interacting with a second spiral and has colors similar to the dropout candidate ($Y_{098} - J_{125} = 1.2$, $J_{125} - H_{160} = 0.35$, $V_{606} - J_{125} = 3.5$), but it is clearly detected in V_{606} . In principle, the Y_{098} -dropout could have been lensed (e.g., see Wyithe et al. 2011), but because of the similar colors with the foreground source, we consider it much more likely that this dropout is part of the foreground system, with its J_{125} -band photometry partially contaminated by emission-line flux (see Atek et al. 2011) and a V_{606} continuum that cannot be detected in the current data assuming its $V_{606} - J_{125}$ is similar to that of the spiral galaxy.

5. THE $z \sim 8$ LBG LUMINOSITY FUNCTION

We derive the completeness, $C(m)$, and magnitude-dependent redshift selection function, $S(z, m)$, of our

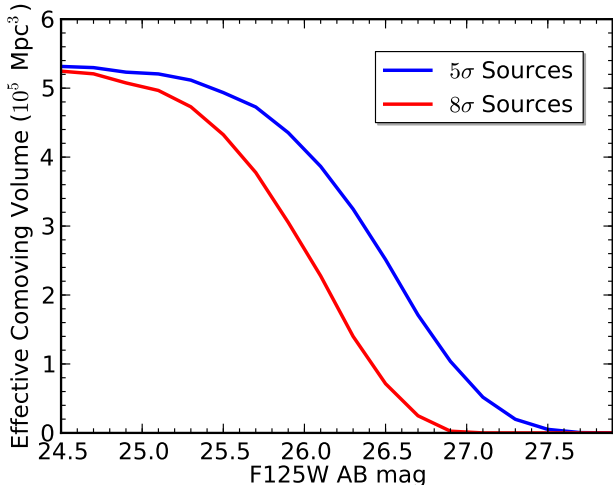


Figure 6. Effective comoving volume for our $z \sim 8$ selection as a function of J_{125} magnitude for both the 5σ (blue) and 8σ (red) source catalogs. The effective volume shown here takes into account reductions from both photometric scatter and incompleteness.

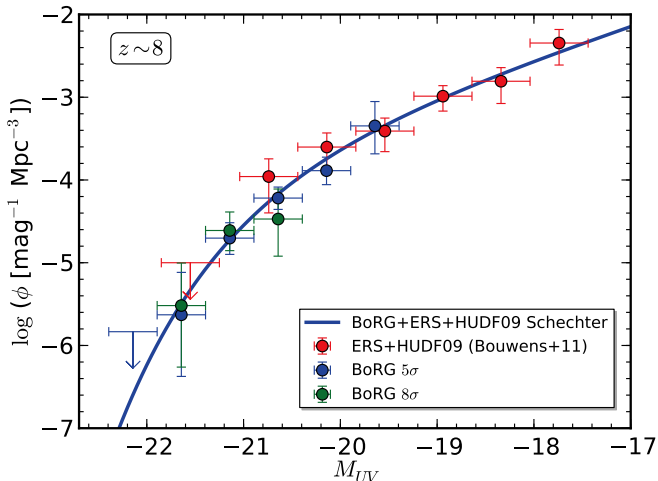


Figure 7. The $z \sim 8$ galaxy UV LF from the current BoRG dataset. The stepwise LFs for our 5σ and 8σ catalogs are shown in blue and green, respectively. The red points represent the stepwise LF derived by Bouwens et al. (2011b) for the ERS+HUDF09 dataset. The blue line is the best-fit Schechter LF from combining the BoRG+ERS+HUDF09 dataset, providing the widest dynamic range in luminosity that is currently available. Our results are consistent with a Schechter form of the UV LF and do not indicate an excess of bright $z \sim 8$ LBGs.

dataset from simulations as described in Oesch et al. (2009, 2012). Briefly, artificial galaxies with a range of spectral energy distributions (SEDs), luminosities, redshifts, and sizes are added to the real images. We then rerun our detection and selection procedure on the data in each individual field to determine both $C(m)$ and $S(z, m)$ (see Figure 5). The simulations are based on $z \sim 4$ galaxy images rescaled to the desired input magnitude and to higher redshift using standard evolutionary relations. In particular we use a size scaling of $(1+z)^{-1}$ as determined from LBGs in the range $z \sim 3-7$ (Ferguson et al. 2004; Bouwens et al. 2004; Oesch et al. 2010) and adopt a UV-continuum slope distribution of $\beta = -2.5 \pm 0.4$, motivated by the recent measurements

Table 7
BoRG Stepwise Determination of the $z \sim 8$ UV LF^a

M_{UV}	ϕ_k (10^{-4} Mpc $^{-3}$ mag $^{-1}$) ^b
-22.14	< 0.015
-21.64	$0.023^{+0.053}_{-0.019}$
-21.14	$0.198^{+0.106}_{-0.072}$
-20.64	$0.604^{+0.217}_{-0.163}$
-20.14	$1.296^{+0.591}_{-0.418}$
-19.64	$4.504^{+4.366}_{-2.434}$

Note. — Assuming $h = 0.7$.

^a For the 5σ sample.

^b The errors are derived from the 68% Bayesian credible intervals for a Poisson distribution.

at $z > 6$ Bouwens et al. (2012); Finkelstein et al. (2011); Dunlop et al. (2012). From these simulations we derive the effective volume for our $z \sim 8$ selection as a function of J_{125} magnitude as shown in Figure 6. By design these simulations take into account the reduction of the effective area and volume probed by the survey because of photometric scatter and presence of foreground sources, including any persistence images in the Y_{098} data. We also note that because we are selecting sources from the J_{125} images, the $J_{125} - H_{160}$ color is not an unbiased measure of the rest-frame UV slope β , so the simulations we perform are crucial to derive the effective volume of our selection, and show that we retain high efficiency, with $S(z, m) \gtrsim 0.8$ (Figure 6).

We construct the stepwise luminosity function from our BoRG observations in 0.5 mag bins for the sample of all 33 Y_{098} -dropouts and for the smaller, but more robust, sample of 8 sources with high S/N ($J_{125} > 8\sigma$) detections. The results are shown in Table 7 and Figure 7 and take into account 34% contamination for the $S/N > 8$ sample and 42% contamination for the $S/N > 5$ sample based on improved estimates following Trenti et al. (2011, 2012b). We take into account the contamination levels of the legacy fields following Oesch et al. (2012) and estimate the BoRG contamination rate by using the Early Release Science (ERS) WFC3/IR data (Windhorst et al. 2011), which also used the F098M filter as the Y band, in combination with the GOODS F606W data degraded to match our relative V_{606} and Y_{098} depths. The main limitation of this approach is the limited area of the ERS data, which is a factor 10 smaller than the BoRG area. Also, we assume that contamination does not vary as a function of luminosity for a given dataset, which is the working assumption of previous studies deriving the LF at high redshift, both in legacy and pure-parallel fields. In principle, the contamination might vary with source brightness, depending on the LF difference for contaminants and $z \sim 8$ galaxies with the same near-IR colors. Without a spectroscopic follow-up survey, and given the lack of confirmed $z \sim 8$ galaxies even in legacy surveys (Schenker et al. 2012; Treu et al. 2012), it is challenging, if at all possible, to investigate this in more detail. Yet, it is reassuring that the spectra of the two BoRG $z \sim 8$ candidates that have been observed at Keck with NIR-CAM by Schenker et al. (2012) and Treu et al. (2012) allow us to exclude the scenario where these sources are $z \sim 1.5$ galaxies with strong emission lines, which are

Table 8
Effect of the Contamination Fraction on the LF
Determination

$1/(1-f)$	$\ln \mathcal{L}$	$\phi_*(10^{-4} \text{ Mpc}^{-3})$	M_*	α
1.0	-24.56	5.6	-20.28	-1.80
1.25	-23.96	4.7	-20.31	-1.90
1.5	-23.84	4.4	-20.29	-1.95
1.73 ^a	-23.98	4.3	-20.26	-1.97
2.0	-24.35	3.8	-20.28	-2.05
2.25	-24.80	3.5	-20.28	-2.10
2.5	-25.31	3.6	-20.23	-2.10

Note. — Assuming $h = 0.7$.

^a Our fiducial value for the contamination correction.

Table 9
Comparison of $z \sim 8$ LF Determinations in the Literature

Reference	$\log \phi_*$ (Mpc^{-3})	M_*	α
This Work	$-3.37^{+0.26}_{-0.29}$	$-20.26^{+0.29}_{-0.34}$	$-1.98^{+0.23}_{-0.22}$
Oesch et al. (2012)	$-3.17^{+0.40}_{-0.55}$	$-19.80^{+0.34}_{-0.57}$	$-2.06^{+0.45}_{-0.37}$
Bouwens et al. (2011b)	$-3.23^{+0.74}_{-0.27}$	-20.10 ± 0.52	-1.91 ± 0.32
Lorenzoni et al. (2011)	-3.0	-19.5	-1.7 (fixed)
Trenti et al. (2011)	-3.4 (fixed)	-20.2 ± 0.3	-2.0 (fixed)
McLure et al. (2010)	-3.46	-20.04 (fixed)	-1.71 (fixed)
Bouwens et al. (2010)	-2.96 (fixed)	-19.5 ± 0.3	-1.74 (fixed)

Note. — Assuming $h = 0.7$.

expected to be the main contaminants of our selection (see Atek et al. 2011 and Trenti et al. 2011).

To explore the effect of contamination in BoRG, we performed the experiment of leaving the contamination fraction as a free parameter in the LF fit, as discussed below (see Table 8). A different contamination fraction would, under our assumptions, simply scale up or down the BoRG LF measurement. Shifting up our data by ~ 0.2 dex, assuming no contamination, can be interpreted very conservatively as an upper limit to the bright end of the $z \sim 8$ galaxy luminosity function. As Figure 7 shows, the low- and high- S/N samples provide a consistent determination of the luminosity function of Y_{098} dropouts in the BoRG dataset and the data in our faintest bins agree with (and are actually slightly lower than) the brightest bins in Bouwens et al. (2011b) from ERS and HUDF09 data. Finally, the measure of a strong clustering signal from the BoRG survey argues against a strong contamination fraction Trenti et al. (2012b).

We derive Schechter function parameters by performing a maximum-likelihood fit to the data, assuming a Poisson distribution of the galaxy number counts in each magnitude bin. Specifically, we maximize the Poisson likelihood for observing N^{obs} sources in a given magnitude bin when N^{exp} are expected to be observed from a given Schechter LF. The likelihood \mathcal{L} is expressed as $\mathcal{L} = \prod_j \prod_i P(N_{j,i}^{obs}, N_{j,i}^{exp})$, where $P(N^{obs}, N^{exp})$ is the Poisson probability distribution and the products are taken over all the fields, j , and magnitude bins, i . To establish the best estimate of the overall shape of the UV LF, we combine our BoRG dataset with those from the deeper ERS+HUDF09 data of Bouwens et al. (2011b), providing the largest dynamic range in luminosity currently possible. Given that the CANDELS observations yield very different preliminary results depending on the

team that analyzed the data to search for $z \sim 8$ galaxies (see Yan et al. 2011a; Oesch et al. 2012), we exclude those data from our analysis.

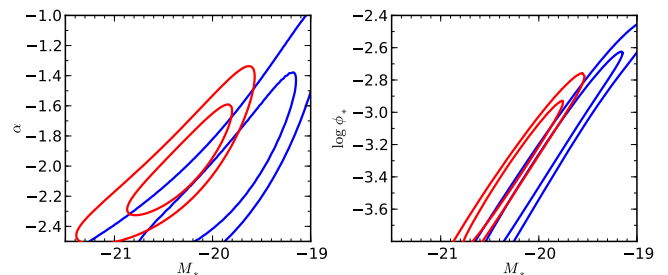


Figure 8. 1σ (68%) and 2σ (95%) confidence intervals in the Schechter LF fit from BoRG+ERS+HUDF data (red lines) compared to the CANDELS+ERS+HUDF determination by Oesch et al. (2012) (blue lines). The BoRG fit has a preference for a marginally brighter M_* , but the two datasets are consistent within their 2σ contours. In particular, we note that our M_* versus α parameter values have much better constraints than the previous studies at $z \sim 8$.

At 68% confidence, for $h = 0.7$ we derive $\phi_* = (4.3^{+3.5}_{-2.1}) \times 10^{-4} \text{ Mpc}^{-3}$, $M_* = -20.26^{+0.29}_{-0.34}$, and a very steep faint-end slope $\alpha = -1.98^{+0.23}_{-0.22}$. As observed in Figure 7, overall the best fit provides a very good description of the data. The covariance in the parameter values is smaller than that in the CANDELS+ERS+HUDF analysis by Oesch et al. (2012) (Yan et al. (2011a) do not fit a LF to their data), but it is still significant, as shown in Figure 8. From this figure it is also clearly evident that our M_* versus α parameter values have much better constraints than previous studies at $z \sim 8$ (Oesch et al. 2012). Formally the bright end of the luminosity function has a marginally low M_* value. However, this is compen-

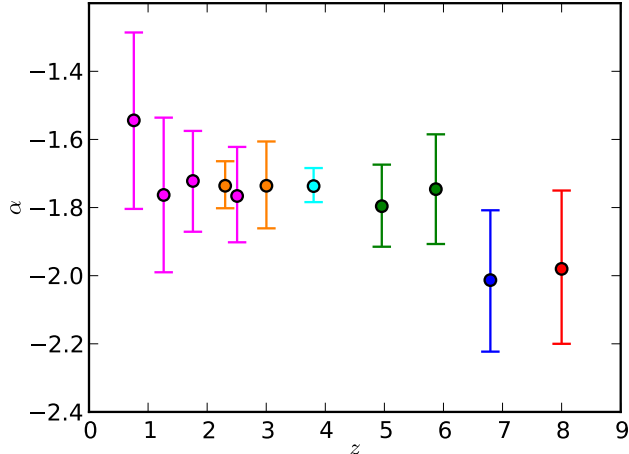


Figure 9. Determination of the Schechter function faint-end slope α for the galaxy LF as a function of redshift. Literature determinations are from Oesch et al. (2010) at $z \sim 0.7 - 2.5$ (magenta), from Reddy & Steidel (2009) at $z \sim 2 - 3$ (orange), from Bouwens et al. (2007) at $z \sim 4$ (cyan), from Bouwens et al. (2012) at $z \sim 5 - 6$ (green), and from Bouwens et al. (2011b) at $z \sim 7$ (blue). Our new determination at $z \sim 8$ is shown in red. All error bars are 1σ (68% confidence). Our latest determination provides some evidence that the LF is becoming steeper at $z \gtrsim 7$, consistent with the $z \sim 7$ measurement.

sated by the low ϕ_* such that the best-fit Schechter function ($\phi_* = 5.9^{+10.1}_{-3.7} \times 10^{-4} \text{ Mpc}^{-3}$, $M_* = -20.1 \pm 0.52$) derived by Bouwens et al. (2011b) is fully consistent with our determination at 68% confidence. As can be seen in Figure 7, the faintest three bins of the BoRG dataset match very closely the brightest bins in Bouwens et al. (2011b). The latest BoRG LF is also very similar to our earlier fit from Trenti et al. (2011), where we had kept ϕ_* and α fixed (see Table 9).

Table 8 shows the impact of varying the contamination fraction f for the BoRG dataset and its associated contamination correction $1/(1-f)$ that is applied to the intrinsic counts per magnitude bin to obtain the estimated observed counts. The table shows that the impact of contamination around our fiducial value $f = 0.42$ is relatively modest. We note that the highest likelihood is associated to a contamination fraction just below our fiducial value, providing indirect evidence to suggest that our derived contamination fraction is robust. Varying the contamination fraction around $f = 0.33$ has almost no impact on the determination of M_* , as the LF is well sampled by the BoRG data in this luminosity range, but affects mostly α ; if we have underestimated f , then the faint-end slope would be even steeper.

As shown in Table 9, our determination of the $z \sim 8$ luminosity function is consistent with previous work (McLure et al. 2010; Lorenzoni et al. 2011; Trenti et al. 2011; Bouwens et al. 2011b; Oesch et al. 2012), taking into account the significant uncertainties in all these measures. Formally, our best fit prefers a low normalization for ϕ_* and a brighter M_* (similar to the $z \sim 7$ value), but the covariance between these parameters is very large (see Figure 9). In particular our BoRG+ERS+HUDF LF fit provides a better constraint on the M_* vs. α parameter uncertainties than the CANDELS+ERS+HUDF determination at $z \sim 8$ Oesch et al. (2012).

In comparing different datasets, it is important to note

that the bright end is still sparsely sampled; for example, the brightest BoRG magnitude bin includes only one source. Therefore, small-number fluctuations are very significant and Poisson noise in the brightest bins can have a large impact on the fit. However, our maximum likelihood fit shows, independent of the M_* versus ϕ_* degeneracy, that the faint-end slope α is being constrained with growing accuracy. Of note, we reduce its 1σ uncertainty at $z \sim 8$ to ± 0.2 and show in Figure 9 that the steepening trend suggested by previous studies (e.g., Bouwens et al. 2011b) is also supported by our LF fit.

The steep faint-end slope derived in our best-fit LF implies that faint galaxies are playing a key role as major producers of ionizing photons. For a Schechter LF, most of the luminosity density contribution is at the faint end (e.g., see left panel of Fig. 3 in Trenti et al. 2010). Furthermore, in the case of $\alpha \sim -2$, there is a logarithmically divergent contribution from sources below the detection limit of the survey. This implies that the total ionizing flux produced by galaxies is sensitive to the exact measure of α (as well as on the extrapolation beyond the detection limit), as shown, for example, in the left panel of Fig. 4 of Bouwens et al. (2012). Assuming that star formation continues to be efficient in lower luminosity galaxies down to $M_{AB} \sim -12$ at $z \sim 8$ (the limit of atomic hydrogen cooling halos, e.g. see Trenti et al. 2010; Finlator et al. 2011), then we expect that the current *HST* observations are only observing $\sim 20\%$ of the light present at $z \sim 8$. A direct proof that we are detecting only the tip of the iceberg of star formation during the epoch of reionization is provided by *HST* observations of high-redshift, spectroscopically confirmed GRBs that have failed to detect host galaxies despite reaching ultrafaint sensitivity ($M_{AB} \sim -17$, see Tanvir et al. 2012). The non-detection of galaxies at locations in the sky where it is confirmed that star formation is happening (because a GRB explosion has occurred) implies that $M_{AB} \gtrsim -15$ galaxies were indeed the main ionizing sources (Trenti et al. 2012a), in full agreement with the interpretation of the LF fit derived in this paper.

Interestingly, our determination of the $z \sim 8$ luminosity function at the bright end is between the debated measurements from the CANDELS dataset obtained by Oesch et al. (2012) and Yan et al. (2011a). However, our data clearly show a well-behaved Schechter function, similar to Oesch et al. (2012), without the unusual shape derived by Yan et al. (2011a). Our LF determination and that by Oesch et al. (2012) are consistent at the $\sim 2\sigma$ level. The observed differences could be partially related to the environment (i.e. cosmic variance (Trenti & Stiavelli 2008)). Oesch et al. (2012) discuss that the ERS measurement by Bouwens et al. (2011b) could have been affected by an overdensity. However, given that the BoRG dataset is not affected by cosmic variance and agrees with Bouwens et al. (2011b), it may well be that the CANDELS-South field is underdense, which would explain the lower M_* value derived from that dataset. The upcoming BoRG observations and those in the CANDELS-North field will help clarify the nature of the discrepancy and provide further improvements to the determination of the bright end of the $z \sim 8$ luminosity function.

6. SUMMARY AND CONCLUSIONS

We present the discovery of 33 Lyman break galaxy (LBG) candidates at $z \sim 8$ detected in *HST*/WFC3 imaging as part of the Brightest of Reionizing Galaxies (BoRG) pure-parallel survey. Our sample of bright Y_{098} -dropout galaxy candidates have J_{125} -band magnitudes between 25.5 and 27.4 mag, obtained from 59 independent lines of sight over a total area of 274 arcmin². The pure-parallel nature of BoRG allows us to obtain an estimate of the galaxy luminosity function which is unaffected by large-scale structure uncertainty and distinct from determinations using legacy surveys limited to a single, or a few, contiguous fields.

With our new data we detect galaxies between $-22 \lesssim M_{AB} \lesssim -19.75$, demonstrating the bright end of the $z \sim 8$ luminosity function is well described by a Schechter form, similar to that found at lower redshifts. Our measurement of the number density of galaxies near the BoRG detection limit ($M_{AB} \sim -20$) is in agreement with the results by Bouwens et al. (2011b). Their measurement is based on ERS+HUDF09 observations that extend to much fainter luminosities, but they lack the area to detect the brighter galaxies at $M_{AB} \lesssim -20.5$ we identify in the BoRG survey. The two datasets are complementary and allow us to obtain the best determination yet of the galaxy luminosity function at $z \sim 8$, with $\phi_* = (4.3^{+3.5}_{-2.1}) \times 10^{-4}$ Mpc⁻³, $M_* = -20.26^{+0.29}_{-0.34}$, and $\alpha = -1.98^{+0.23}_{-0.22}$ for $h = 0.7$.

Covariance in the parameters, albeit reduced thanks to the increase in the dynamic range of the fit, is still very significant. However, this affects primarily M_* versus ϕ_* . We find that our BoRG+ERS+HUDF LF fit provides a better constraint on the M_* versus α parameter uncertainties than the CANDELS+ERS+HUDF determination at $z \sim 8$ Oesch et al. (2012). The faint-end slope uncertainty is starting to be reduced to a point where there is a hint of steepening compared to $z \lesssim 6$. This steepening is expected based on numerical and theoretical models of galaxy formation in the epoch of reionization (Trenti et al. 2010; Jaacks et al. 2012). As a consequence of this large abundance of faint galaxies, it is expected that such systems will dominate the total star formation rate and ionizing photon production (Shull et al. 2012), which has recently been confirmed observationally by the non-detection of host galaxies in a sample of six $z > 5$ Gamma-Ray Bursts (Trenti et al. 2012a; Tanvir et al. 2012). Our determination of a steep α for a Schechter fit of the LF is robust against our estimate of the contamination fraction of the BoRG survey ($f = 0.42$ for the 5σ sample); as shown in Table 8, if f were higher, α would be steeper. In the near future, the upcoming ultra-deep observations of GO 12498 (PI Ellis) will improve the determination of the number density of the faintest galaxies observable by *HST*, while scheduled BoRG and CANDELS-North observations will further increase the search area for the brightest galaxies at $z \sim 8$, allowing us to further tighten the constraints on the LF.

The $z \sim 8$ candidates identified here are good targets for follow-up observations from ground and space observatories. We have started a spectroscopic campaign to confirm their redshift, to measure the distribution of Ly α equivalent width (which is related to the IGM ionization state), and also to rule out contamination from

emission-line galaxies at $z \sim 1.5$ (Treu et al. 2012). The availability of multi-object spectrographs both on Keck (MOSFIRE) and Gemini South (FLAMINGOS-2), will enable faster progress, especially in fields that have overdensities of sources similar to the protocluster candidate we reported in Trenti et al. (2012b). In addition, the brightest BoRG sources are expected to have star formation rates of $10 - 20 M_\odot \text{ yr}^{-1}$ based on their rest-frame UV luminosity, making them prime targets for ALMA observations as they are expected to fall well within the telescope sensitivity based on the Carilli et al. (2008) predictions. If these candidates are spectroscopically confirmed, this would allow us to possibly extend the detection of [C II] 158 μm , high- J CO emission lines, and perhaps dust emission as well, to $z \sim 8$, after the recent record established at $z = 7.1$ from a QSO host galaxy (Venemans et al. 2012). Finally, *Spitzer*/IRAC observations, combined with spectroscopic redshifts, would also be very useful to quantify the rest-frame optical properties of these sources before the advent of the *James Webb Space Telescope*.

The Space Telescope Science Institute is operated by AURA Inc., under NASA contract NAS5-26555. This work was supported by grants HST-GO-11563, HST-GO-11700, and HST-GO-12572. This work included coordinated parallel data taken as part of the COS GTO program (PI Green). Support for PO was provided by NASA through Hubble Fellowship grant HF-51278.01. JS acknowledges support from grant NNX08-AC14G. MT gratefully acknowledges the hospitality of the Kavli Institute for Theoretical Physics, where part of this research was carried out with support by the National Science Foundation under Grant No. PHY11-25915. Part of the work presented in this paper was performed by MT and TT while attending the program “First Galaxies and Faint Dwarfs: Clues to the Small Scale Structure of Cold Dark Matter” at the Kavli Institute of Theoretical Physics at the University of California Santa Barbara.

REFERENCES

- Atek, H., Siana, B., Scarlata, C., et al. 2011, *ApJ*, 743, 121
 Bertin, E., & Arnouts, S. 1996, *A&AS*, 117, 393
 Bouwens, R. J., Illingworth, G. D., Blakeslee, J. P., Broadhurst, T. J., & Franx, M. 2004, *ApJ*, 611, L1
 Bouwens, R. J., Illingworth, G. D., Franx, M., & Ford, H. 2007, *ApJ*, 670, 928
 Bouwens, R. J., Illingworth, G. D., Oesch, P. A., et al. 2010, *ApJ*, 708, L69
 Bouwens, R. J., Illingworth, G. D., Labbe, I., et al. 2011a, *Nature*, 469, 504
 Bouwens, R. J., Illingworth, G. D., Oesch, P. A., et al. 2011b, *ApJ*, 737, 90
 —. 2012, *ApJ*, 752, L5
 Bradley, L. D., Bouwens, R. J., Zitrin, A., et al. 2012, *ApJ*, 747, 3
 Carilli, C. L., Walter, F., Wang, R., et al. 2008, *Ap&SS*, 313, 307
 Dunlop, J. S., McLure, R. J., Robertson, B. E., et al. 2012, *MNRAS*, 420, 901
 Ferguson, H. C., Dickinson, M., Giavalisco, M., et al. 2004, *ApJ*, 600, L107
 Finkelstein, S. L., Papovich, C., Salmon, B., et al. 2011, *ArXiv e-prints*, 1110.3785
 Finlator, K., Oppenheimer, B. D., & Davé, R. 2011, *MNRAS*, 410, 1703
 Grogin, N. A., Kocevski, D. D., Faber, S. M., et al. 2011, *ApJS*, 197, 35

- Hall, N., Bradač, M., Gonzalez, A. H., et al. 2012, *ApJ*, 745, 155
- Jaacks, J., Choi, J.-H., Nagamine, K., Thompson, R., & Varghese, S. 2012, *MNRAS*, 420, 1606
- Knapp, G. R., Leggett, S. K., Fan, X., et al. 2004, *AJ*, 127, 3553
- Koekemoer, A. M., Fruchter, A. S., Hook, R. N., & Hack, W. 2002, in *The 2002 HST Calibration Workshop : Hubble after the Installation of the ACS and the NICMOS Cooling System*, ed. S. Arribas, A. Koekemoer, & B. Whitmore, 337
- Koekemoer, A. M., Faber, S. M., Ferguson, H. C., et al. 2011, *ApJS*, 197, 36
- Lorenzoni, S., Bunker, A. J., Wilkins, S. M., et al. 2011, *MNRAS*, 414, 1455
- Malhotra, S., Rhoads, J. E., Pirzkal, N., et al. 2005, *ApJ*, 626, 666
- McLure, R. J., Dunlop, J. S., Cirasuolo, M., et al. 2010, *MNRAS*, 403, 960
- McLure, R. J., Dunlop, J. S., de Ravel, L., et al. 2011, *MNRAS*, 418, 2074
- Oesch, P. A., Carollo, C. M., Stiavelli, M., et al. 2009, *ApJ*, 690, 1350
- Oesch, P. A., Bouwens, R. J., Carollo, C. M., et al. 2010, *ApJ*, 725, L150
- Oesch, P. A., Bouwens, R. J., Illingworth, G. D., et al. 2012, *ArXiv e-prints*, 1201.0755
- Oke, J. B. 1974, *ApJS*, 27, 21
- Ono, Y., Ouchi, M., Mobasher, B., et al. 2012, *ApJ*, 744, 83
- Postman, M., Coe, D., Benítez, N., et al. 2012, *ApJS*, 199, 25
- Reddy, N. A., & Steidel, C. C. 2009, *ApJ*, 692, 778
- Robertson, B. E. 2010, *ApJ*, 713, 1266
- Ryan, R. E., Thorman, P. A., Yan, H., et al. 2011, *ApJ*, 739, 83
- Schechter, P. 1976, *ApJ*, 203, 297
- Schenker, M. A., Stark, D. P., Ellis, R. S., et al. 2012, *ApJ*, 744, 179
- Schlegel, D. J., Finkbeiner, D. P., & Davis, M. 1998, *ApJ*, 500, 525
- Shull, J. M., Harness, A., Trenti, M., & Smith, B. D. 2012, *ApJ*, 747, 100
- Stark, D. P., Ellis, R. S., & Ouchi, M. 2011, *ApJ*, 728, L2
- Steidel, C. C., Giavalisco, M., Dickinson, M., & Adelberger, K. L. 1996, *AJ*, 112, 352
- Tanvir, N. R., Levan, A. J., Fruchter, A. S., et al. 2012, *ApJ*, 754, 46
- Trenti, M., Perna, R., Levesque, E. M., Shull, J. M., & Stocke, J. T. 2012a, *ApJ*, 749, L38
- Trenti, M., & Stiavelli, M. 2008, *ApJ*, 676, 767
- Trenti, M., Stiavelli, M., Bouwens, R. J., et al. 2010, *ApJ*, 714, L202
- Trenti, M., Bradley, L. D., Stiavelli, M., et al. 2011, *ApJ*, 727, L39
- . 2012b, *ApJ*, 746, 55
- Treu, T., Trenti, M., Stiavelli, M., Auger, M. W., & Bradley, L. D. 2012, *ApJ*, 747, 27
- van Dokkum, P. G. 2001, *PASP*, 113, 1420
- Venemans, B. P., McMahon, R. G., Walter, F., et al. 2012, *ApJ*, 751, L25
- Willott, C. J., Delorme, P., Reylé, C., et al. 2010, *AJ*, 139, 906
- Windhorst, R. A., Cohen, S. H., Hathi, N. P., et al. 2011, *ApJS*, 193, 27
- Wyithe, J. S. B., Yan, H., Windhorst, R. A., & Mao, S. 2011, *Nature*, 469, 181
- Yan, H., Finkelstein, S. L., Huang, K.-H., et al. 2011a, *ArXiv e-prints*, 1112.6406
- Yan, H., Yan, L., Zamojski, M. A., et al. 2011b, *ApJ*, 728, L22
- Zheng, W., Postman, M., Zitrin, A., et al. 2012, *ArXiv e-prints*, 1204.2305